Journal of Membrane Science 658 (2022) 120712

Contents lists available at ScienceDirect

Journal of Membrane Science

journal homepage: www.elsevier.com/locate/memsci

A novel IL/MOF/polymer mixed matrix membrane having superior CO_2/N_2 selectivity

Nitasha Habib [a,b], Ozce Durak [a,b], Muhammad Zeeshan [a,b], Alper Uzun [a,b,c,**], Seda Keskin [a,b,*]

[a] Department of Chemical and Biological Engineering, Koç University, Rumelifeneri Yolu, 34450, Sariyer, Istanbul, Turkey
[b] Koç University TÜPRAŞ Energy Center (KUTEM), Koç University, Rumelifeneri Yolu, 34450, Sariyer, Istanbul, Turkey
[c] Koç University Surface Science and Technology Center (KUYTAM), Koç University, Rumelifeneri Yolu, 34450, Sariyer, Istanbul, Turkey

ARTICLE INFO

Keywords:
Mixed matrix membranes (MMMs)
Metal organic framework (MOF)
Ionic liquid (IL)
IL/CuBTC composite
CO_2 separation

ABSTRACT

In this work, we synthesized an ionic liquid (IL)/metal organic framework (MOF) composite, 1-ethyl-3-methylimidazolium acetate/copper-1,3,5-benzenetricarboxylate ([EMIM][OAc]/CuBTC) and used it as a filler in a polymer, Pebax, to fabricate novel IL/MOF/polymer mixed matrix membranes (MMMs). CuBTC/Pebax and [EMIM][OAc]/CuBTC/Pebax MMMs having different filler loadings of 10, 15, and 20 wt.% were prepared by solution casting method and characterized using various techniques including X-ray diffraction (XRD), scanning electron microscopy (SEM), infrared spectroscopy (IR), and thermogravimetric analysis (TGA). Uniform dispersion of MOF and IL/MOF fillers in the MMMs was observed. Incorporation of IL/MOF composite into Pebax significantly improved CO_2 permeability and CO_2/N_2 selectivity of the polymer by 2.5- and 5.5-times, respectively. Gas permeability measurements showed that the MMM having 15 wt.% IL/MOF loading exhibits significantly higher CO_2 permeability of 335 Barrer and CO_2/N_2 selectivity of 176 than the Pebax membrane having CO_2 permeability of 135 Barrer and CO_2/N_2 selectivity of 32. CO_2/N_2 selectivity of the [EMIM][OAc]/CuBTC/Pebax MMM with 15 wt.% [EMIM][OAc]/CuBTC filler loading was the highest among the selectivity values reported for other types of IL/MOF/polymer MMMs in the literature. All the CuBTC/Pebax MMMs and [EMIM][OAc]/CuBTC/Pebax MMMs that we fabricated in this work exceeded the Robeson's updated upper bound, showing the excellent potential of these novel membranes for CO_2/N_2 separation.

1. Introduction

Membrane technology has been proven to be promising due to its low installation cost, operational simplicity, high-energy efficiency, and environmental friendliness. Polymer membranes can be easily fabricated [1], however, their gas separation performances are restricted by the well-known Robeson's upper bound [2], which represents the trade-off between the gas permeability and selectivity for a target gas separation. Mixed matrix membranes (MMMs), composed of inorganic fillers dispersed in the polymer matrix, have received significant interest in the last decade since they combine easy processability of polymers with the good gas separation performance of inorganic fillers. Traditionally, zeolites have been used as fillers for the fabrication of zeolite/polymer MMMs, however, difficulty of preparing defect-free zeolite crystals and poor adhesion between the polymer and zeolite particles limit the applicability of these MMMs [3].

Metal-organic frameworks (MOFs), a relatively new family of novel organic-inorganic materials, have been recently used as fillers in MMMs to enhance the gas separation performance of polymer membranes [4–8]. MOFs have high surface areas, large porosities, controllable pore sizes, good mechanical and thermal stabilities. The most important advantage of MOFs over other traditional fillers is that their physical and chemical properties can be easily tuned by choosing the proper metal-ligand pair for a target application [9,10]. A large number of experimental studies has been reported on MOF/polymer MMMs for various gas separation applications including CO_2/CH_4, CO_2/N_2, H_2/CO_2 [11–15]. Incorporation of MOFs into polymers generally improve either the gas permeability or the selectivity of the polymer membrane [16]. For instance, Nafisi et al. [17] fabricated ZIF-8/Pebax MMMs and the MMM with 35 wt.% ZIF-8 loading showed significantly higher CO_2 permeability (1287 Barrer) compared to pure polymer (351 Barrer) whereas CO_2/CH_4 (32) and CO_2/N_2 (9) selectivities of the

* Corresponding author. Department of Chemical and Biological Engineering, Koç University, Rumelifeneri Yolu, 34450, Sariyer, Istanbul, Turkey.
** Corresponding author. Department of Chemical and Biological Engineering, Koç University, Rumelifeneri Yolu, 34450, Sariyer, Istanbul, Turkey.
E-mail addresses: auzun@ku.edu.tr (A. Uzun), skeskin@ku.edu.tr (S. Keskin).

https://doi.org/10.1016/j.memsci.2022.120712
Received 26 March 2022; Received in revised form 9 May 2022; Accepted 5 June 2022
Available online 7 June 2022
0376-7388/© 2022 The Authors. Published by Elsevier B.V. This is an open access article under the CC BY-NC-ND license (http://creativecommons.org/licenses/by-nc-nd/4.0/).

membrane remained unchanged. On the other hand, incorporation of a MOF could increase the selectivity of a polymer at the expense of decreased gas permeabilities. For example, Ordonez et al. [18] reported improved H_2/CO_2 and CO_2/CH_4 selectivities with increasing ZIF-8 loading for ZIF-8/Matrimid MMMs, from 121 to 472 and from 40 to 124, respectively, compared to the pure Matrimid membrane. Whereas, the CO_2, H_2, and CH_4 permeabilities were decreased from 12 to 7, 29 to 20, and 0.3 to 0.1 Barrer, respectively. Therefore, improving both the gas permeability and selectivity of the polymer membranes simultaneously by addition of new and novel filler materials is still highly desired.

Ionic liquids (ILs) can enhance the separation performance of MOFs due to their high affinity towards various gasses, such as CO_2, in addition to modifying the MOFs' pore structure. Incorporation of ILs into MOFs to prepare IL/MOF composites can combine the advantages of both constituents, such as high affinity of ILs towards desired gas molecules and tunable structure of both materials [19,20]. IL/MOF composites have proven to be highly CO_2 selective over N_2 and CH_4 gasses through adsorption studies which leads to improved selectivities compared to pristine MOFs [21–26]. Therefore, utilization of IL/MOF composites in MMM applications has been examined and recent studies showed that IL/MOF composites can significantly improve the selectivity of the membranes depending on the well-controlled location of IL molecules [27,28].

Introduction of ILs into MMMs via confining them into the pores of MOFs modifies the pore structures and chemical properties of the designed composite filler. For instance, Ban et al. [29] incorporated [BMIM][Tf_2N]/ZIF-8 composite ([BMIM][Tf_2N]:1-butyl-3-methylimidazolium bis(trifluoromethylsulfonyl)imide) into polysulfone (PSf) and the resulting MMM having a volume fraction of 6% IL/ZIF-8 showed improved CO_2/CH_4 and CO_2/N_2 selectivities (from 19 to 38 and from 29 to 116, respectively) compare to pure PSf. Li et al. [30] incorporated a similar composite, [BMIM][Tf_2N]/ZIF-8, into Pebax and the resulting MMM with 15 wt.% IL/ZIF-8 loading showed significant increase in CO_2/CH_4 and CO_2/N_2 selectivities (from 20 to 34 and from 48 to 84, respectively). Yasmeen et al. [31] investigated the separation performance of [APTMS][OAc]/ZIF-67/PSf MMM ([APTMS][OAc]: 3-(trimethoxysilyl)propan-1-aminium acetate) and showed that CO_2/CH_4 and CO_2/N_2 selectivities of the MMM with 30 wt.% IL/MOF filler loading are higher (72.1 and 74.5, respectively) than the selectivities of the pure PSf membrane (25.1 and 27.2, respectively).

IL/MOF composites have been incorporated into highly permeable polymers, such as polymers of intrinsic microporosity (PIM-1) and less permeable polymers, such as Matrimid, to synthesize IL/MOF/polymer MMMs with improved gas separation performance. Chen et al. [27] incorporated [BMIM][Tf_2N]/MOF-801 composite into PIM-1. The CO_2 permeability of IL/MOF/PIM-1 MMM with 5 wt.% IL/MOF loading was 2.2-times higher (9420 Barrer) than that of PIM-1 membrane (4110 Barrer) and CO_2/N_2 selectivity (29) was 1.4-times higher compared to that of PIM-1 membrane (20). Ferreira et al. [28] incorporated, 1-propyl-3-methylimidazolium bromide, [PMIM][Br]/MIL101(Cr) composite into Matrimid and the IL/MOF/polymer MMMs exhibited CO_2 permeability of 44 Barrer, which was 4-times higher than that of pure Matrimid (9.8 Barrer). Lin et al. [32] synthesized [EMIM][Tf_2N]/CuBTC composite ([EMIM][Tf_2N]:1-ethyl-3-methylimidazolium bis(trifluoromethylsulfonyl)imide) and prepared IL/MOF/polymer MMMs by incorporating the composite into 6FDA polymer. Results showed that CO_2 permeability of IL/CuBTC/polymer MMM was significantly higher, 1200 Barrer, than the pure polymer membrane, 790 Barrer. However, CO_2/N_2 and CO_2/CH_4 selectivities of the MMM were only slightly improved compared to that of the pure polymer. These results highlight that IL/MOF composites can be highly promising filler particles for MMM applications due to their high CO_2 affinities. Thus, the synthesis of new IL/MOF composites and their use in polymers to generate MMMs can lead to new membranes with exceptional CO_2 separation performances. Accordingly, extending the list of such filler materials having different components, ILs and MOFs, is highly desired to understand how their structures should be tuned for improved separation performance of the MMMs. Besides, these initial studies have also shown that using fillers improved the gas permeability and/or the gas selectivity of the polymer membrane. Enhancing both the gas permeability and selectivity to exceed the Robeson's upper bound has been the main target of all the MMM studies for a very long time.

In this work, we reported a novel IL/MOF/polymer MMM offering an exceptionally high performance for CO_2/N_2 separation. Considering the very large variety and number of possible IL/MOF/polymer combinations, this work will significantly contribute into the design and development of new MMMs having different types of IL/MOF fillers. 1-ethyl-3-methylimidazolium acetate, [EMIM][OAc], was incorporated in CuBTC by wet impregnation method to synthesize [EMIM][OAc]/CuBTC composite. [EMIM][OAc] was selected as the IL due to its high CO_2 solubility associated with its Lewis basic acetate anion [20]. CuBTC was chosen as the porous support for the newly synthesized IL/MOF composite considering the limited number of studies on IL/CuBTC/-polymer MMMs [32]. These selected IL and CuBTC were used to prepare a novel [EMIM][OAc]/CuBTC composite for utilizing the potential of these individual constituents in CO_2/N_2 separation. Then, [EMIM][OAc]/CuBTC composite was dispersed as a filler in Pebax at the loadings of 10, 15, and 20 wt.% to prepare [EMIM][OAc]/CuBTC/Pebax MMMs. Pebax was selected as a polymer matrix for its well-known affinity for polar gases [33], with the aim of fabricating highly CO_2 selective MMMs demonstrating enhanced filler-polymer compatibility. Synthesized [EMIM][OAc]/CuBTC composite, CuBTC/Pebax MMMs, and [EMIM][OAc]/CuBTC/Pebax MMMs were characterized in deep detail using various characterization techniques, including X-ray diffraction (XRD), scanning electron microscopy (SEM), Infrared spectroscopy (IR), thermogravimetric analysis (TGA), and corresponding structural changes were discussed. Single-component adsorption isotherms of CO_2 and N_2 for pristine CuBTC and [EMIM][OAc]/CuBTC composite were experimentally measured using volumetric adsorption method and single-component CO_2 and N_2 permeability of all MMMs were measured using a custom-built constant pressure/variable volume setup. Consequently, we evaluated the gas permeability and selectivity of the MMMs containing CuBTC and [EMIM][OAc]/CuBTC fillers by comparing their results with previously reported MOF/polymer and IL/MOF/polymer MMMs. The results of this work will significantly contribute into the literature of MMMs and accelerate the design and development of new IL/MOF/polymer MMMs in near future.

2. Experimental methods

2.1. Materials

CuBTC (Basolite C300), [EMIM][OAc], analytical grade ethanol and acetone were purchased from Sigma-Aldrich. Pebax 1657 was kindly provided by Arkema. Each chemical was stored in an Argon-filled Labconco glovebox. The gases used in the permeation experiment, CO_2 (99.9%), N_2 (99.998%), and He (99.999%) were purchased from Air Liquide.

2.2. Synthesis of IL/MOF composite

[EMIM][OAc]/CuBTC composite was prepared via wet impregnation method with 30 wt.% IL loading. The wetness limit of CuBTC was determined as 30 wt.% and the IL loading in the IL/CuBTC composite was set to wetness limit to obtain the maximum possible selectivity enhancement [20]. Pristine CuBTC was activated at 105 °C under vacuum before the IL incorporation. Firstly, 0.3 g of IL was mixed in 20 ml of acetone and left under stirring for 1 h to obtain a homogenous solution. Afterwards, 0.7 g of freshly activated CuBTC was added into the solution, and the mixture was stirred at 35 °C in an open atmosphere to slowly evaporate the solvent. After the complete evaporation of the

solvent, resulting composite was placed in oven at 105 °C for 12 h for further drying. IL-incorporated CuBTC composite was obtained and stored in the desiccator.

2.3. Fabrication of MMMs

All the membranes were fabricated by the solution-casting technique [34]. Before fabricating the membranes, MOF, polymer pellets, and IL/MOF composite were oven dried at 80 °C overnight to remove any trapped moisture. The neat Pebax membrane was prepared with 4 wt.% polymer solution in a water/ethanol mixture (30/70) followed by continuous stirring for 4 h at 80 °C. The solution was casted on a Teflon substrate and controlled evaporation was carried out for 48 h. Further traces of residual solvent were removed by drying the membrane at 65 °C for 12 h.

The optimum filler loading in MMMs was carefully chosen in a range from 10 to 20 wt.% since a uniform dispersion of the filler particles in the polymer matrix is challenging to achieve at higher filler loadings [18,35–37]. Moreover, a decrease in the separation performance of the MMMs was observed when the filler loading was increased beyond 15 wt.%, thus, we set the maximum filler loading as 20 wt.%, a loading meaningfully higher than 15 wt.%, to confirm reaching the maxima in performance. Various loadings of CuBTC and [EMIM][OAc]/CuBTC composite (10, 15, and 20 wt.%) were dispersed in an ethanol/water solvent mixture and stirred continuously for 12 h. For the fabrication of MOF/polymer MMMs, the solution vessels were then placed in an ultra-sonication bath for 0.5 h to ensure well dispersion of the MOF. In the next step, the polymer pellets were stirred in water/ethanol mixture (30/70) for 4 h at 80 °C and mixed with prepared solution of the MOF particles, followed by 0.5 h sonication. The solutions were continuously stirred for 4 h and then casted on a Teflon substrate.

IL/MOF/polymer MMMs were prepared by following a similar above-mentioned procedure. Typically, IL/MOF loadings of 10, 15, and 20 wt.% were dispersed in an ethanol/water solvent mixture, stirred continuously for 12 h followed by ultra-sonication. After this step, the IL/MOF suspension was dried at 70 °C and IR spectra was analyzed to be sure about the structural integrity of the used IL/MOF composite. The IR spectra showed no change in the peak of IL/MOF composite, before and after mixing in ethanol/water mixture and maintained its original structure as shown in Fig. S1 of the Supplementary Data (SD). Moreover, washing experiments for IL/CuBTC were performed to check if leaching of the IL might happen during the synthesis of IL/MOF/polymer MMM. IL/CuBTC sample was washed three-times with ethanol/water mixture and the filtrate was collected in a vial. After washing, the composite was dried at 105 °C. The IR spectra of the composite before and after washing, the filtrate, pristine CuBTC and IL are presented in Fig. S2. Accordingly, the IR spectrum of the filtrate lacks features associated with the IL, whereas the spectra of the washed and dried sample preserved the features related with the IL. These results confirmed that leaching of IL during IL/MOF/polymer MMM synthesis is unlikely to happen. After these confirmations, the sonicated IL/MOF solution was added to Pebax solution, stirred for 4 h, and casted on a Teflon substrate. The residual solvent of all the casted membranes was dried by placing an inverted funnel on the petri dishes for 24 h. Membranes were dried in an oven, peeled off from the substrate carefully and stored in a desiccator. The average thickness of MMMs was measured using a digital slide caliper as 70–100 μm.

2.4. Characterization techniques

X-ray diffraction (XRD) analysis of pristine CuBTC, [EMIM][OAc]/CuBTC composite and [EMIM][OAc]/CuBTC/Pebax MMMs were obtained by using a Bruker D8 Advance instrument with Cu-Kα radiation ($\lambda = 1.5406$ Å) in the 2θ range between 5 and 50° with a step size of 0.0204°. Infrared spectroscopy (IR) spectra were collected using a Bruker Vertex 80v spectrometer in the range of 400 cm^{-1} to 4000 cm^{-1} and at a spectral resolution of 2 cm^{-1} in transmittance mode. Deconvolution of peaks was performed using Fityk software by employing the Voigt function [38]. The surface area and pore volume of the filler particles were determined by N_2 adsorption isotherms obtained at −196 °C and the pressure range of 10^{-6} to 1 bar using a Micromeritics ASAP 2020. Pristine MOF and IL/MOF composite samples were degassed at 150 °C under vacuum for 12 h before the measurements. The Brunauer-Emmett-Teller (BET) equation and the *t*-plot method were used to calculate surface area and pore volume of the pristine MOF and IL/MOF composite, in the pressure range of P/P_0:0.05–0.65.

A Zeiss Evo LS 15 electron microscope was utilized to examine the cross-sectional morphologies of MMMs. All membrane samples were prepared by freeze cutting under liquid N_2, followed by a coating of the gold layer. Scanning electron microscope (SEM) images of all the membrane samples were obtained at a magnification of 10 k × under an ultra-high vacuum with an accelerating voltage of 20 kV. Thermogravimetric analyses (TGA) were performed using TA Instruments Q500 analyzer under an inert atmosphere using N_2 as purge and balance gas at 60 and 40 mL/min, respectively. The experiments were performed starting from room temperature up to 800 °C with a heating rate of 10 °C min^{-1}. The onset (T_{onset}) and derivative onset (T'_{onset}) temperatures were determined from the thermogravimetric (TG) and derivative TG (DTG) curves, respectively. The T'_{onset} values were considered as the temperature point at which the thermal decomposition initiated, as the T_{onset} values generally overestimate the thermal decomposition temperatures. CO_2 and N_2 gas solubilities in bulk [EMIM][OAc] were determined by COnductor like Screening MOdel for Realistic Solvents (COSMO-RS) calculations [39]. COSMOThermX software version C30_160 was utilized between the pressure range of 0.001 and 1 bar with respective triple-z valence polarized basis set (TZVP-FINE) parameterizations.

2.5. Gas adsorption measurements

A volumetric gas sorption analyzer, iSorb HP2, Quantachrome, was utilized to measure CO_2 and N_2 adsorption isotherms of pristine CuBTC and [EMIM][OAC]/CuBTC composite. Approximately, 0.45 g of the samples were used for each measurement. First, each sample was degassed for 12 h under a high vacuum at 125 °C. Adsorption isotherms were obtained at 25 °C in the pressure range of 0.01–1 bar. Each adsorption isotherm was fitted to the Dual-site Langmuir-Freundlich model and Langmuir-Freundlich model by using Ideal Adsorbed Solution Theory $(IAST)^{++}$ software [40] and the corresponding fitting parameters were given in Table S1.

2.6. Gas permeation experiments

MMMs were tested for the permeability of pure CO_2 and N_2 gases using a custom-built constant pressure/variable volume setup. The instrumental setup for performing gas permeability measurements by using He as a sweep gas is shown in Fig. 1. Each membrane was tested three-times to ensure the reliability of the permeability measurements and an average of the permeability values was reported along with the relative standard deviation.

MMMs were placed in stainless steel module containing two separate compartments with effective surface area of 7 cm^2 and they were tightly sealed by rubber O-rings. The composition and flowrate of each gas were controlled by electronic mass flow controllers (MFCs, Alicat) and the upstream pressure was controlled with a back pressure regulator (BPR, Equilibar). During the experiments, the upstream pressure was maintained at 1 bar and the downstream side was under atmospheric pressure. All measurements were made at 35 °C and controlled by a temperature controller (Ordel, SC771) having a temperature stability of ±5 °C. He was flowed continuously in the permeate side of the cell as a sweep gas and periodically to the feed side to purge the gases present in the system after the experiment was finished. The outlet gas composition

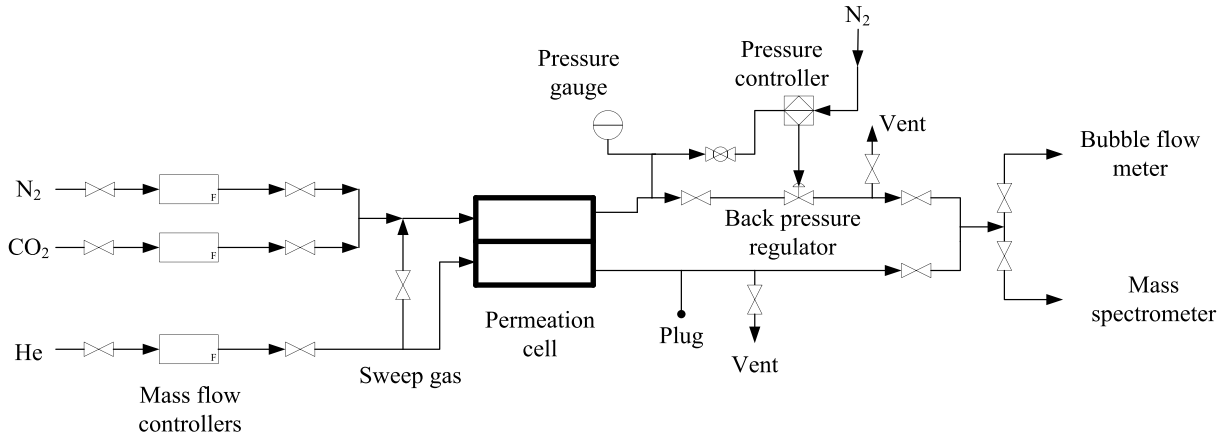


Fig. 1. Schematic diagram of the gas permeation setup.

was analyzed by Hiden Analytical, QGA mass spectrometer equipped with a quadrupole mass filter and a heated sampling capillary. The CO_2 and N_2 fluxes were calculated from the sweep gas flow rate and the permeate composition was determined via the mass spectrometric analysis of the permeate/sweep stream. The permeability of the membranes for gas i, P_i (Barrer), was calculated by using the following equation (1), where J_i is the flux (cm^3(STP)/s), ΔP_i (cmHg) is the transmembrane pressure difference and l (cm) is the membrane thickness measured by digital vernier calipers:

$$P_i = (l \times J_i) / \Delta P_i \quad (1)$$

The ideal selectivity of the membrane (S_{CO_2/N_2}) was calculated by dividing the permeability values measured for different gases as follows:

$$S_{CO_2/N_2} = P_{CO_2} / P_{N_2} \quad (2)$$

3. Results and Discussions

3.1. Characterization of the materials

3.1.1. IL/MOF composite

Surface area and pore volume of the pristine CuBTC and the [EMIM][OAc]/CuBTC composite were determined by the N_2 adsorption isotherms presented in Fig. S3. Results demonstrated that both pristine CuBTC and [EMIM][OAc]/CuBTC composite have typical type-I adsorption isotherms, a characteristic feature of microporous materials. Thus, we inferred that CuBTC maintains its microporosity upon the IL incorporation. Results further showed that the BET surface area and pore volume of CuBTC decreased from 1152 m^2/g and 0.13 cm^3/g to 9.12 m^2/g and 0.03 cm^3/g upon the incorporation of [EMIM][OAc], respectively. These significant decreases indicated that the pores of CuBTC were mostly occupied by the [EMIM][OAc] molecules, confirming the successful incorporation of IL into MOF, consistent with the literature [19,41]. However, it is noteworthy that overall N_2 uptake is also dependent on the solubility of N_2 in the ILs. To address this issue, additional COSMO-RS calculations were conducted to compute the solubility of N_2 in bulk [EMIM][OAc] at the BET measurement conditions as given in Fig. S4. Results demonstrated that N_2 has almost negligible solubility in [EMIM][OAc] at the BET measurement conditions. Therefore, it can be inferred that some IL molecules located at the gate openings of the CuBTC might restrict the accessibility of N_2 into the completely/partially available pores [42,43]. Therefore, BET analysis can be quantitatively misleading in terms of providing reliable data for IL/MOF composites.

XRD diffraction patterns of pristine CuBTC and [EMIM][OAc]/CuBTC composite are presented in Fig. 2. The presence of main

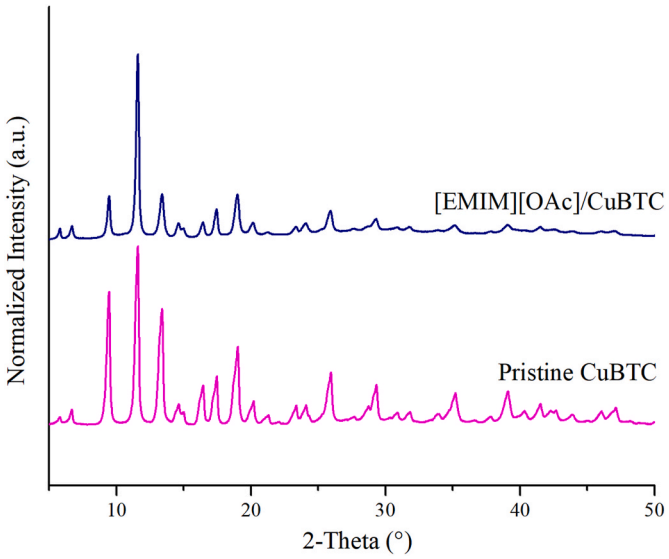


Fig. 2. XRD spectra of pristine CuBTC and [EMIM][OAc]/CuBTC composite.

diffraction peaks at 6.7, 9.4, and 11.6° in both diffraction data confirmed that IL incorporation did not affect the crystalline structure of CuBTC. However, some minor differences in the peak intensities were observed in XRD patterns of CuBTC and [EMIM][OAc]/CuBTC composite, which are likely associated with the changes in the electronic environment of the crystals or their preferential orientation due to the presence of IL molecules inside the pores [29,44]. Moreover, morphology of the pristine CuBTC and [EMIM][OAc]/CuBTC composite was investigated using the SEM images and Fig. S5 demonstrated that the surface morphology of CuBTC remained mostly intact upon the incorporation of [EMIM][OAc], consistent with an earlier report presenting a composite of CuBTC with 1-butyl-3-methylimidazolium tetrafluoroborate, [BMIM][BF_4] [45].

Fig. 3 represents the TGA analysis of CuBTC, [EMIM][OAc], and [EMIM][OAc]/CuBTC. In the TGA curves, two weight loss steps were observed for CuBTC and bulk IL. The initial weight loss between 80 and 100 °C is associated with the moisture content of the structure. Accordingly, CuBTC decomposed approximately at T'_{onset} value of 320 °C, which may be attributed to the removal of the organic linker and decomposition of CuBTC structure [46]. The bulk IL decomposed through a typical one-step decomposition mechanism with T'_{onset} value of approximately 190 °C, whereas the IL/MOF composite showed a T'_{onset} of approximately 260 °C. These results demonstrated that

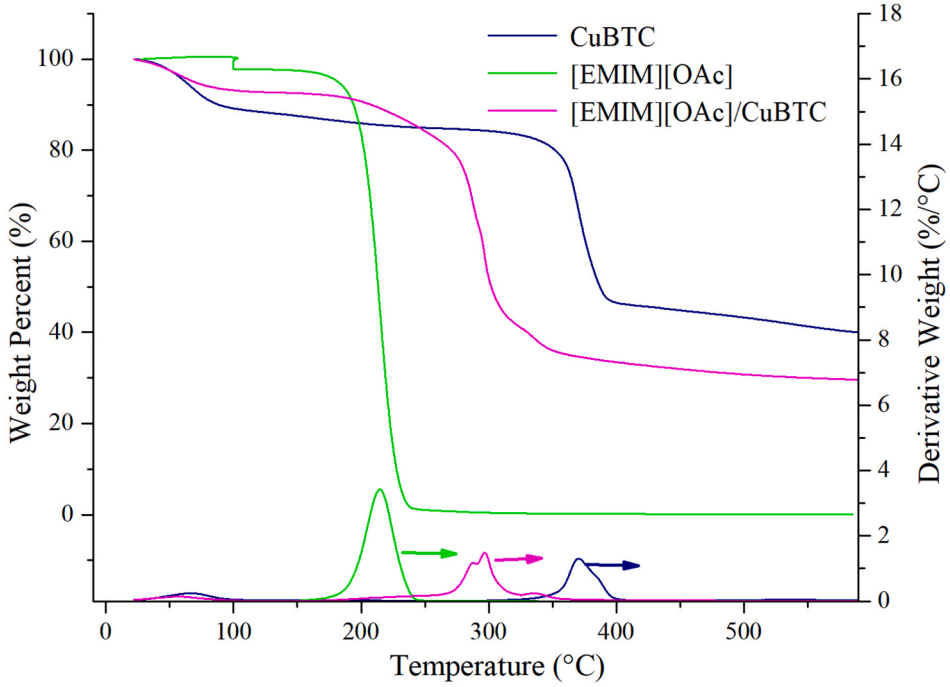


Fig. 3. TGA and DTG curves of CuBTC, [EMIM][OAc]/CuBTC, and bulk [EMIM][OAc].

synthesized IL/MOF composite has a higher T'_{onset} compared to the bulk IL. This change in T'_{onset} can be attributed to the presence of direct IL-MOF interactions in the composite offering a completely different behavior of the IL when incorporated into CuBTC, consistent with the previous reports [47].

To have further insights into the interactions between IL and CuBTC, IR analysis was performed. The IR spectra of pristine CuBTC, bulk [EMIM][OAc], and [EMIM][OAc]/CuBTC composite are shown in Fig. 4. The peaks were deconvoluted, and then the shifts in the peak positions were determined compared to the corresponding characteristic peak positions in the bulk [EMIM][OAc] and pristine CuBTC. In [Emim][OAc] spectrum, the peaks located at 1570, 1429 and 1232 cm^{-1} represented the ν(C═O), $\delta(CH_3)$ and ν(C–CH_3) vibrational modes due to the presence of acetate ion in the IL, whereas the peaks at 1185 and 1377 cm^{-1} were attributed to ν(C–N) and ν(C–O) vibrations of the imidazolium ring present in $[EMIM]^+$ cation [48]. It was observed that ν(C–N)

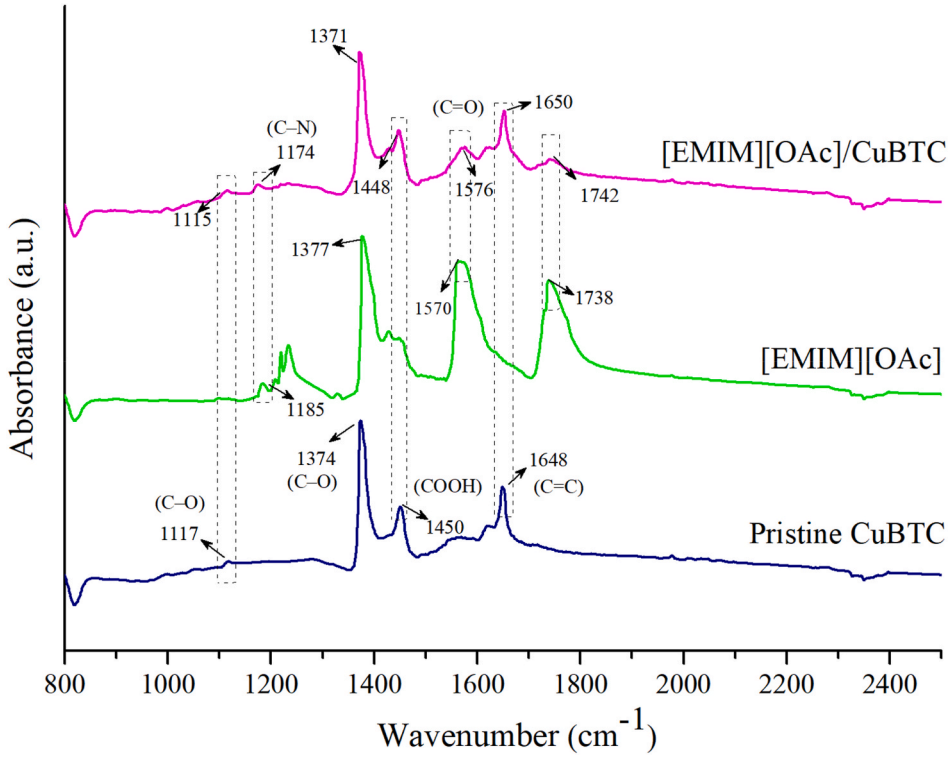


Fig. 4. FTIR spectra of pristine CuBTC, [EMIM][OAc]/CuBTC, and bulk [EMIM][OAc].

and ν(C–O) characteristic vibrations of the imidazolium ring exhibited red-shifts of 11 and 6 cm^{-1}, respectively, in the IR spectra of IL/CuBTC suggesting a molecular interaction between CuBTC and the cation of IL [49]. The presence of shifts in the IL band positions indicated that the IL was successfully incorporated inside the CuBTC cages.

In pristine CuBTC, the IR bands from 1300 to 1700 cm^{-1} can be associated with the carboxylate linker and were attributed to the coordination of benzenetricarboxylate (BTC) linker to the copper sites. Accordingly, the peaks located at 1648, 1450, and 1374 cm^{-1} correspond to the ν(C═C), the asymmetric ν(COOH) and ν(C–O) vibrations, respectively, of benzene groups in the BTC linker [50]. The characteristic ν(C–O–Cu) and ν(C–C) peaks of CuBTC, located at 1117 and 1450 cm^{-1} [35], slightly red shifted to lower wavenumbers with 2 cm^{-1}, upon the incorporation of IL, similar with the previously reported IL/CuBTC studies [45,51]. These red shifts in the characteristic ν(C–O–Cu) and ν(C–C) bands of pristine CuBTC imply a possible change in the electronic environment of existing pores and can be attributed to the presence of IL molecules which may weakened the Cu–O bond of CuBTC. Hence, observed changes in the characteristic peak positions of bulk IL and pristine CuBTC can be inferred to the electron sharing between the cation of IL and the open metal sites of CuBTC, confirming the presence of direct interactions between IL and MOF in the composite material. Moreover, IR results were consistent with the TGA analysis confirming the presence of interactions between IL and CuBTC.

3.1.2. Characterization of MMMs

MOF/polymer MMMs and IL/MOF/polymer MMMs were synthesized by incorporating 10, 15, and 20 wt.% loadings of pristine CuBTC and [EMIM][OAc]/CuBTC as fillers into Pebax. SEM analysis was used to investigate the dispersion of CuBTC and the effect of incorporation of IL-modified CuBTC into the polymer matrix. Cross sectional morphologies of CuBTC/polymer MMMs and IL/CuBTC/polymer MMMs are presented in Fig. 5(a–c) and (d-f), respectively. These images presented the almost defect-free and dense structure of all MMMs. All the MMMs

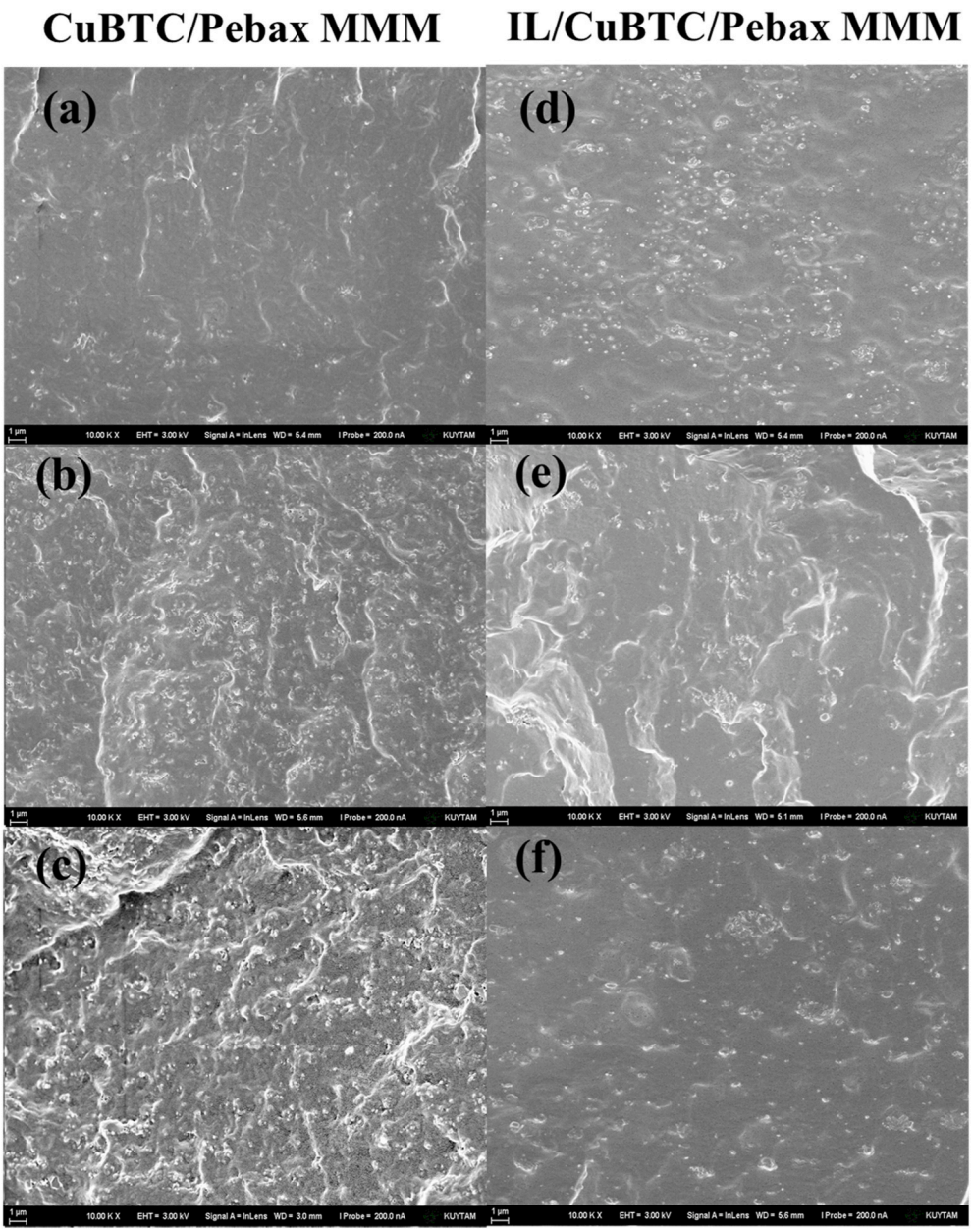


Fig. 5. Cross-sectional SEM images of CuBTC/Pebax MMMs (given in (a), (b), and (c)) and [EMIM][OAc]/CuBTC/Pebax MMMs (given in (d), (e), and (f)) with corresponding filler amounts for both types of MMMs are (a, d) 10 wt.%, (b, e) 15 wt.%, (c, f) 20 wt.% at a magnification of 10 k ×.

became less smooth as the filler loading was increased from 10 to 20 wt. %. More uniform and smooth structure was observed for IL/CuBTC/polymer MMM in Fig. 5(d–f) compared to the MOF/polymer MMMs in Fig. 5(a–c). This structural uniformity was attributed to the decreased amount of CuBTC in the case of IL/CuBTC/polymer MMMs. Overall, no macro-scale voids were observed in the magnified SEM images presented in Fig. 5, however, filler particles showed slight agglomeration at high loading of 20 wt.%, which can be attributed to the non-uniform dispersion of filler particles at high loadings.

The EDS results of Cu mapping also proved the uniform dispersion of the filler particles represented in Fig. S6. The Cu distribution in CuBTC/Pebax MMMs became more prominent as the CuBTC loading was increased from 10 to 20 wt.%, shown in Figs. S6(a–c). In the case of [EMIM][OAc]/CuBTC/Pebax MMMs shown in Figs. S6(d–f), it was observed that IL addition leads to more dense and smooth membranes compared to MOF/polymer MMMs, which may be attributed to the reduction in the crystallinity of the membranes [52].

XRD patterns of pure Pebax, CuBTC/Pebax MMMs, and [EMIM][OAc]/CuBTC/Pebax MMMs with 10, 15, and 20 wt.% fillers are represented in Fig. 6. A broad peak at 13–23° and a narrow peak at 24.2° were observed in the pure polymer as shown in Fig. 6(a), which were attributed to the polyamide (PA) group, representing the semicrystalline structure of Pebax [53]. For all the MMMs, the positions of these peaks remain almost the same, indicating that the intersegmental spacing of Pebax did not change with the filler incorporation. Furthermore, XRD spectra presented in Fig. 6(b–g) showed new peaks at 6.7, 9.4, and 11.7° corresponding to the characteristic peaks of CuBTC in all MMMs [54]. It was also observed that as the CuBTC loading was increased from 10 to 20 wt.%, the intensities of the corresponding CuBTC peaks were also increased as shown in Fig. 6(b–d), indicating that the crystal structure of CuBTC remains intact in the polymer. However, in the case of IL/CuBTC/Pebax MMMs shown in Fig. 6(e–g), the intensity of PA peaks of the polymer was decreased as the [EMIM][OAc]/CuBTC loading was increased, which can be ascribed to the disruption of polymer chains packing and reduced crystallinity of the membranes [55].

The TGA curves of CuBTC/Pebax MMMs and [EMIM][OAc]/CuBTC/Pebax MMMs at different filler loadings are shown in Fig. 7(a–c) and (d-f), respectively. The decomposition temperatures did not change significantly with the increase in the filler loadings. The first stage of the weight loss was observed around 80–90 °C, caused by the desorption of water and the residual solvent. At the second stage, the mass loss around 260–270 °C indicated the decomposition of organic ligands of CuBTC and [EMIM][OAc]/CuBTC composite present in CuBTC/Pebax MMMs and [EMIM][OAc]/CuBTC MMMs, respectively. The third stage of weight loss was primarily due to the decomposition of the polymer backbone, which is at the range of 300 ± 5 °C for CuBTC/Pebax MMMs and at the range of 360 ± 5 °C for [EMIM][OAc]/CuBTC/Pebax MMMs. The decomposition temperature of [EMIM][OAc]/CuBTC/Pebax MMMs was observed to be slightly higher than that of CuBTC/Pebax MMMs, which was attributed to the high thermal stability of [EMIM][OAc]/CuBTC composite, consistent with the literature [56]. In general, all the MMMs are stable up to 300 °C, indicating that they can withstand high temperatures.

FTIR spectra of pure Pebax, CuBTC/Pebax MMMs, and [EMIM][OAc]/CuBTC/Pebax MMMs with 10, 15, and 20 wt.% loadings of CuBTC and [EMIM][OAc]/CuBTC, respectively, are represented in Fig. 8 (a–g). In the IR spectra of Pebax as shown in Fig. 8(a), the characteristic peaks of PA group located at 3297, 1637, and 1732 cm^{-1} were attributed to the hydrogen bonded ν(N–H) group [57,58], (O–C–O) group, and (H–N–C═O) group [59], respectively. The peak observed near 1100 cm^{-1} related to the (C–O–C) group was attributed to the (PEO) part of the Pebax [60]. Moreover, the δ(C–H) and ν(C–H) vibrations at 2864-2942 cm^{-1} and 1440 cm^{-1} represented the aliphatic groups present in Pebax. Similar characteristic peaks of Pebax were observed in all MMMs as shown in Fig. 8(b–g). CuBTC/Pebax MMMs with 10 wt.% CuBTC loading given in Fig. 8(b) showed characteristic peaks of Pebax, located at 1116 cm^{-1} (C–O–C), 1636 cm^{-1} (O–C–O), 1738 cm^{-1} (H–N–C═O), 3298 cm^{-1} (N–H) and 2866–2942 cm^{-1}(C–H). As the loading of CuBTC was increased to 15 and 20 wt.%, (O–C–O) exhibited blue-shifts of 3 and 6 cm^{-1} and (C–O–C) exhibited red-shifts of 6 and 5

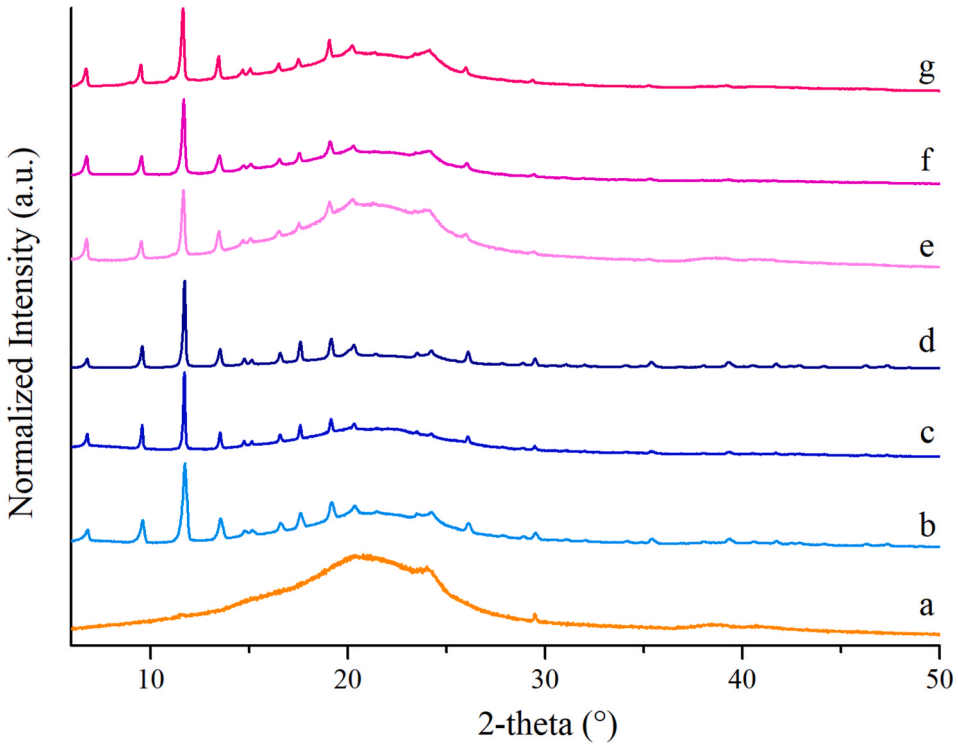


Fig. 6. XRD spectra of (a) pure Pebax, (b) CuBTC/Pebax MMMs with 10 wt.%, (c) 15 wt.%, (d) 20 wt.% CuBTC loadings and (e) [EMIM][OAc]/CuBTC/Pebax MMMs with 10 wt.%, (f) 15 wt.%, (g) 20 wt.% [EMIM][OAc]/CuBTC loadings.

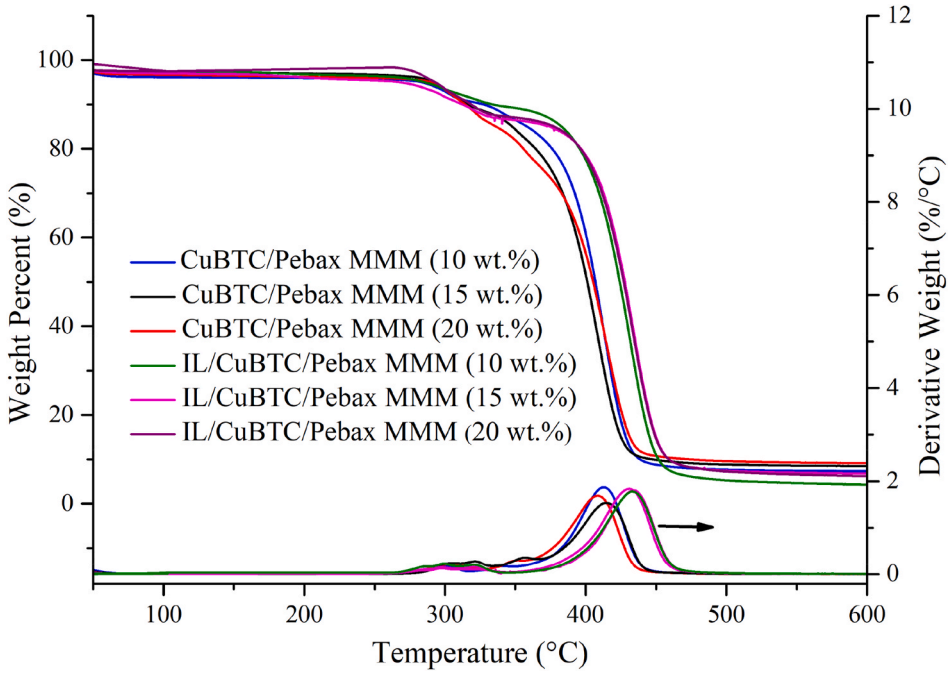


Fig. 7. TGA and DTG curves of CuBTC/Pebax MMMs with (a) 10 wt.%, (b) 15 wt.%, (c) 20 wt.% CuBTC loadings and [EMIM][OAc]/CuBTC/Pebax MMMs with (d) 10 wt.%, (e) 15 wt.%, (f) 20 wt.% [EMIM][OAc]/CuBTC loadings.

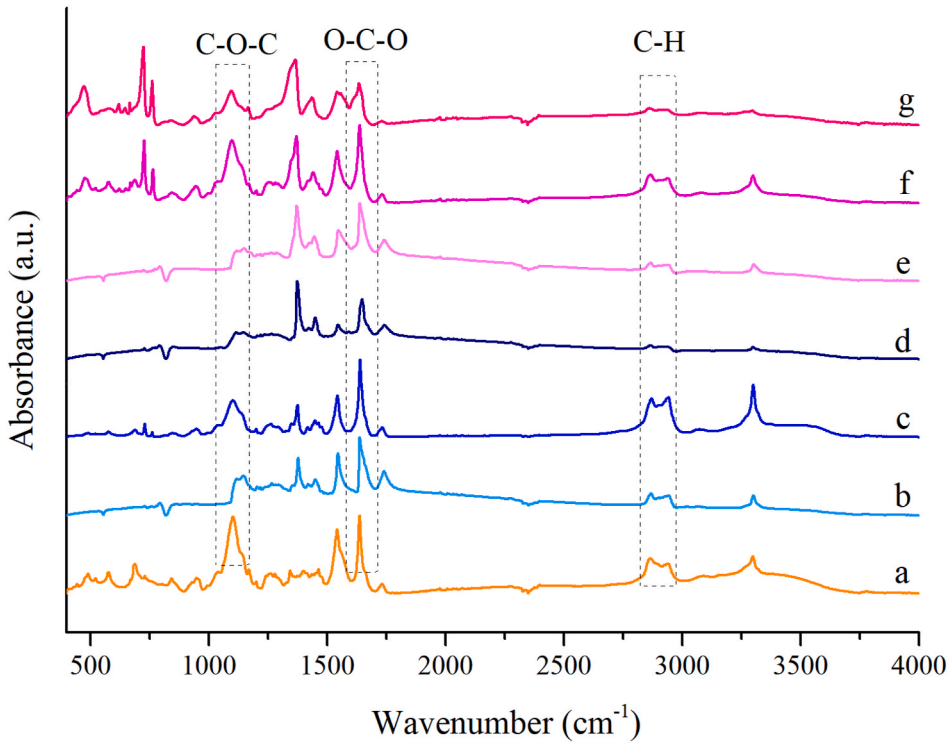


Fig. 8. IR spectra of (a) pure Pebax, CuBTC/Pebax MMMs with (b) 10 wt.%, (c) 15 wt.%, (d) 20 wt.% CuBTC loadings, and [EMIM][OAc]/CuBTC/Pebax MMMs with (e) 10 wt.%, (f) 15 wt.%, (g) 20 wt.% [EMIM][OAc]/CuBTC loadings.

cm^{-1}, respectively. These shifts suggested the presence of the interaction between the CuBTC and Pebax. Moreover, the new peaks observed at 729 cm^{-1} (C–H bending vibrations) and 1377 cm^{-1} (COO symmetric vibrations) can be associated with the characteristic peaks of CuBTC and, consistently, the peak intensities were increased with the increasing CuBTC loading.

The IR spectra of [EMIM][OAc]/CuBTC/Pebax MMMs are represented in Fig. 8(e–g). At 10 wt.% IL/CuBTC loading, in Fig. 8(e), the spectra showed characteristic peaks of Pebax located at 1107 cm^{-1} (C–O–C), 1640 cm^{-1} (O–C–O), 1738 cm^{-1} (H–N–C═O), 3301 cm^{-1} (N–H) and 2866–2936 cm^{-1}(C–H). As the loading of IL/CuBTC composite was increased to 15 and 20 wt.%, it was observed that (O–C–O) exhibited red-shifts of 4 and 5 cm^{-1} and, (C–O–C) exhibited red-shifts of 10 and 11 cm^{-1}, respectively. These shifts suggested the interaction

present between IL/CuBTC composite and Pebax. Moreover, the peaks located at 727 cm^{-1} (C–H bending vibrations) and 1370 cm^{-1} (COO symmetric vibrations) corresponding to the characteristic peaks of CuBTC were observed to be intensified with the increase in IL/CuBTC loadings and this could be explained by the increase in CuBTC concentration. In contrast, as the CuBTC and IL/CuBTC loadings were increased from 10 to 20 wt.%, the intensity of IR bands corresponding to (C–H) and (C–O–C) groups of Pebax was observed to decrease as shown in Fig. 8(c, d, f, g), indicating agglomeration of the filler particles and polymer chain rigidification at high loadings [61].

3.2. Gas separation performance of materials

3.2.1. IL/MOF composite

Single-component volumetric adsorption measurements of CO_2 and N_2 gases in CuBTC and [EMIM][OAc]/CuBTC composite were performed up to 1 bar at 25 °C as shown in Fig. 9(a). Results showed that both CO_2 and N_2 uptakes decreased upon IL incorporation into CuBTC. For instance, CO_2 and N_2 uptakes of CuBTC at 1 bar, corresponding to 91.3 and 5.8 cm^3/g, decreased to 11.4 and 0.9 cm^3/g, respectively, in the case of IL/CuBTC composite. The decrease in the gas uptakes was attributed to the reduced surface area and pore volume of the [EMIM][OAc]/CuBTC composite considering the occupation of pores of CuBTC by the IL molecules.

The corresponding ideal CO_2/N_2 selectivities of pristine CuBTC and IL/CuBTC composite were calculated from the single-component gas adsorption data and shown in Fig. 9(b). Data illustrated that IL/CuBTC composite is more CO_2 selective than its CuBTC counterpart, at low-pressure region up to 0.2 bar. Upon the incorporation of [EMIM][OAc], the ideal CO_2/N_2 selectivity of CuBTC was increased to 122.6 (67.3) from 20.3 (20.2) at 0.001 (0.01) bar yielding 6-times (3.3-times) improvement. Table S1 compares [EMIM][OAc]/CuBTC adsorption selectivity results with those reported for other IL/CuBTC composites in the literature. The ideal CO_2/N_2 selectivity of [EMIM][OAc]/CuBTC composite that we synthesized is 1.6-times higher (67.3 at 0.01 bar and 25 °C) than that of 1-ethyl-3-methylimidazolium diethyl phosphate, [EMIM][DEP]/CuBTC composite (42.3 at 0.01 bar and 25 °C), showing the high potential of [EMIM][OAc]/CuBTC composite for selective CO_2 separation from N_2 [51]. As demonstrated in Fig. 9(b), above 0.2 bar, a decrease in the selectivity of the composite was observed compared to the pristine material. This decrease can be explained by the change in the driving forces of surface adsorption with increasing pressure. In the low-pressure range, gas adsorption is significantly determined by the adsorbent's affinity towards the guest molecules [26,62], however, with increasing pressure, the adsorption mechanism mostly depends on the available pore volume of the material. Therefore, the reduced selectivity of the composite observed above 0.2 bar can be attributed to the change in the adsorption mechanism from surface affinity to pore availability. Overall, these results illustrated that the [EMIM][OAc]/CuBTC composite is highly CO_2 selective at low pressures and can have a huge potential as a filler material for MMMs to achieve CO_2/N_2 separation with high selectivity.

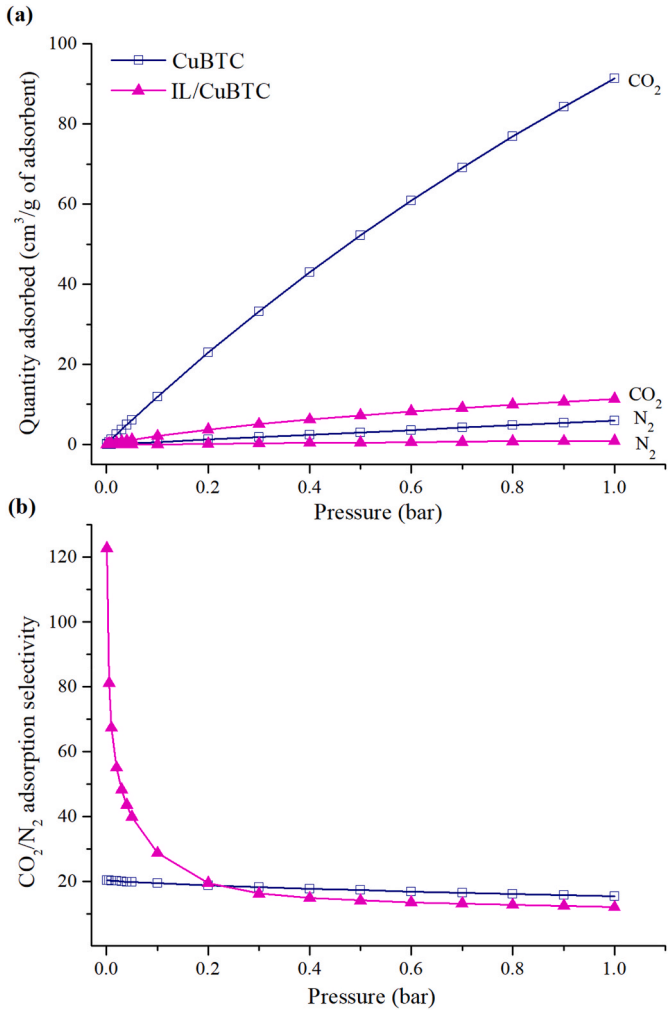


Fig. 9. (a) CO_2 and N_2 adsorption isotherms, (b) ideal CO_2/N_2 selectivity of pristine CuBTC and [EMIM][OAc]/CuBTC composite at 25 °C in the pressure range between 0.001-1 bar.

3.2.2. MOF/polymer and IL/MOF/polymer MMMs

We examined gas permeabilities and selectivities of CuBTC/Pebax MMMs and [EMIM][OAc]/CuBTC/Pebax MMMs. Single-component gas permeation tests were conducted at 35 °C and 1 bar for both MMMs. Fig. 10(a) and (b) show CO_2 permeabilities and CO_2/N_2 permeation selectivities of CuBTC/Pebax MMMs and [EMIM][OAc]/CuBTC/Pebax MMMs with different CuBTC and IL/CuBTC loadings, respectively. The data for CO_2 and N_2 permeability and CO_2/N_2 selectivity is also presented in Table S3. For pure Pebax membrane, CO_2 and N_2 permeabilities were measured as 134.6 ± 2 and 4.2 ± 0.5 Barrer, respectively and CO_2/N_2 selectivity was calculated as 31.8 ± 1.7. For CuBTC/Pebax MMMs having 10 wt.% CuBTC loading, CO_2 and N_2 permeabilities were measured as 190 ± 4 and 2.67 ± 1.1 Barrer, respectively, leading to a CO_2/N_2 selectivity of 71 ± 11. These results show that upon the incorporation of CuBTC at a filler loading of 10 wt.%, CO_2 permeability of the membrane increased, whereas N_2 permeability decreased, resulting in an improved CO_2/N_2 selectivity. CO_2 permeability was further increased to 286 ± 9 Barrer and N_2 permeability was decreased to 2.22 ± 0.4 Barrer as the CuBTC loading was increased to 15 wt.%. As a result, CuBTC/Pebax MMMs having 15 wt.% CuBTC loading exhibited a CO_2/N_2 selectivity of 128 ± 11. Overall, CO_2 permeabilities of CuBTC/Pebax MMMs with 10 and 15 wt.% CuBTC loadings were 1.4- and 2.1-times higher than the pure Pebax membrane. Moreover, CO_2/N_2 selectivities of CuBTC/Pebax MMMs with 10 and 15 wt.% CuBTC loadings were also 2.2- and 4-times higher compared to the selectivity of the pure polymer membrane. These results showed that incorporation of CuBTC as a filler into Pebax to synthesize CuBTC/Pebax MMMs resulted in a significantly improved CO_2/N_2 selectivity.

We then compared CO_2/N_2 separation performance of CuBTC/Pebax MMM with the other MOF/Pebax MMMs reported in the literature. For example, UiO-66/Pebax MMM having 10 wt.% UiO-66 loading was reported to have CO_2 permeability of 96 Barrer at 25 °C and 3 bar [63]. Thus, CuBTC/Pebax MMM that we synthesized in this work has 2-times higher permeability than UiO-66/Pebax MMM. The CO_2/N_2 selectivity of CuBTC/Pebax MMM was 1.2-times higher (71) than the highest reported CO_2/N_2 selectivity (56.5) of UiO-66/Pebax MMM. We also compared the separation performance of CuBTC/Pebax MMM with the data reported at 23 °C and 1 bar for ZIF-8/Pebax MMM having various

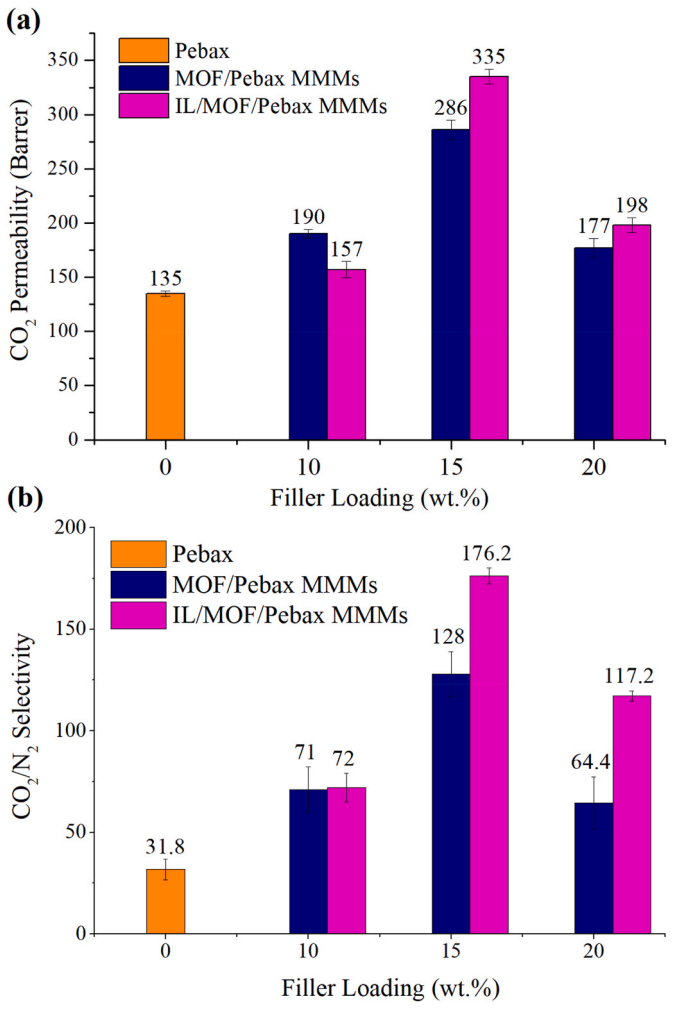


Fig. 10. (a) CO_2 permeability, (b) CO_2/N_2 selectivity of CuBTC/Pebax MMMs with 10, 15, and 20 wt.% CuBTC loadings, and [EMIM][OAc]/CuBTC/Pebax MMMs with 10, 15, and 20 wt.% [EMIM][OAc]/CuBTC loadings measured at 35 °C and 1 bar.

ZIF-8 loading [52]. CO_2 permeability and CO_2/N_2 selectivity of CuBTC/Pebax MMM having 15 wt.% CuBTC loading were 2.8- and 3.6-times higher, respectively, compared to the highest CO_2 permeability (100 Barrer) and CO_2/N_2 selectivity (35) of ZIF-8/Pebax MMM having 15 wt.% ZIF-8 loading. A more detailed comparison of CuBTC/Pebax MMMs with the other MMMs reported in the literature is given in Table S4. Results illustrated that the CO_2 permeabilities and CO_2/N_2 selectivities of CuBTC/Pebax MMMs presented in this study are superior compared to the literature. Overall, the significant enhancement we observed in CO_2 permeability of the MMM upon the CuBTC addition can be attributed to the increased free volume in the polymer matrix due to increased CuBTC loading [64], and the strong CO_2 affinity of open Cu^{+2} sites of CuBTC framework [8].

Separation performance of the polymer membrane was further improved when the [EMIM][OAc]/CuBTC composite was used as the filler. For IL/MOF/polymer MMMs with 10 wt.% IL/CuBTC loading, CO_2 and N_2 permeabilities were measured as 157.5 ± 7.5 and 2.19 ± 0.2 Barrer, respectively, leading to a CO_2/N_2 selectivity of 71.9 ± 7. The CO_2 permeability was further increased to 335 ± 7 Barrer and the N_2 permeability was decreased to 1.90 ± 0.3 Barrer as the IL/CuBTC loading was increased to 15 wt.%. As a result, IL/CuBTC/Pebax MMMs having 15 wt.% IL/CuBTC loading exhibited a CO_2/N_2 selectivity of 176.3 ± 4. This result shows that upon the incorporation of IL/CuBTC at a loading of 10 wt.% and 15 wt.%, CO_2 permeability of the membrane increased whereas N_2 permeability decreased, resulting in an improved CO_2/N_2 selectivity. Overall, CO_2 permeabilities of IL/CuBTC/Pebax MMMs with 10 and 15 wt.% CuBTC loadings were 1.1- and 2.5-times higher than the Pebax membrane. Moreover, CO_2/N_2 selectivities of IL/CuBTC/Pebax MMMs with 10 and 15 wt.% IL/CuBTC loadings were also 2.2- and 5.5-times higher compared to the selectivity of the pure polymer membrane.

These improvements in the gas separation performance of IL/MOF/polymer MMMs synthesized in this study were mainly attributed to the high CO_2 affinity of the acetate ion present in the IL, which significantly enhanced the CO_2/N_2 selectivity [65]. Furthermore, the introduction of IL into the pores of CuBTC prior to membrane fabrication resulted in a significant reduction in the pore volume of composite and improved its molecular sieving effect [30]. Since CO_2 has a smaller kinetic diameter (3.3 Å) compared to the that of N_2 (3.64 Å), preferential permeation of CO_2 over N_2 was favored in IL/MOF/polymer MMMs, leading to improved CO_2/N_2 selectivities. When the excessive amount of filler, 20 wt.%, was incorporated into polymer, a dramatic decrease in both CO_2 permeability and CO_2/N_2 selectivity was observed as shown in Fig. 10(a and b), which can be attributed to the reduced compatibility between the filler and the polymer at higher loadings and agglomeration of the filler particles [18,27,66]. These changes (i.e., agglomeration) in the morphology of the IL/MOF/polymer MMMs and MOF/polymer MMMs at higher filler loadings were also observed in the SEM images given in Fig. 5. Despite this, no large aggregates were observed in the membrane, helping to avoid the interfacial defects between the filler and polymer.

CO_2 permeability and CO_2/N_2 selectivity data of the CuBTC/Pebax MMMs and [EMIM][OAc]/CuBTC/Pebax MMMs are shown in Fig. 11 together with the Robeson's upper bound [10]. To make a comprehensive evaluation of the MMMs that we introduced in this work, we collected the data for other MOF/polymer MMMs and IL/MOF/polymer MMMs for CO_2/N_2 separation from the literature and showed them in Fig. 11 and listed their properties in Table S4. The literature data were collected in the pressure and temperature range of 1–6 bar and 20–35 °C, respectively. CuBTC/Pebax MMMs with 10, 15, and 20 wt.% CuBTC loadings and [EMIM][OAc]/CuBTC/Pebax MMMs with 10, 15, and 20 wt.% [EMIM][OAc]/CuBTC loadings surpassed the upper bound by outperforming many other MMMs for CO_2/N_2 separation.

We compared the separation performance of [EMIM][OAc]/CuBTC/Pebax MMM that we fabricated, with [BMIM][Tf_2N]/ZIF-8/Pebax MMM having an IL/MOF loading of 15 wt.% [30]. CO_2 permeability of [EMIM]

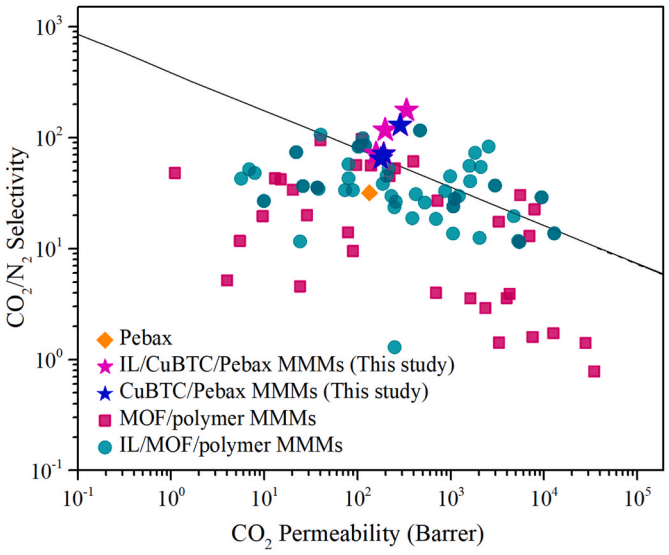


Fig. 11. Comparison of CO_2/N_2 selectivity and CO_2 permeability of MMMs synthesized in this study with the literature data. The line represents the Robeson's upper bound [2].

[OAc]/CuBTC/Pebax MMM (335 Barrer) was 3-times higher than that of [BMIM][Tf_2N]/ZIF-8/Pebax MMM (105 Barrer), under the same temperature (35 °C) and pressure conditions (1 bar). Moreover, the CO_2/N_2 selectivity of [EMIM][OAc]/CuBTC/Pebax MMM (176.2) was also 2-times higher than the reported CO_2/N_2 selectivity (84.5) of [BMIM][Tf_2N]/ZIF-8/Pebax MMM. We also compared the separation performance of [EMIM][OAc]/CuBTC/Pebax MMM with 1-butyl-3-methylimidazolium hexafluorophosphate, [BMIM][PF_6]/ZIF-8/Pebax MMMs, reported at 3 bar and 35 °C [67]. CO_2 permeability of [EMIM][OAc]/-CuBTC/Pebax MMM was 2.9-times higher than that of [BMIM][PF_6]/ZIF-8/Pebax MMM (120 Barrer), and CO_2/N_2 selectivity was also 2.2-times higher, compared to the best reported selectivity (85) of [BMIM][PF_6]/ZIF-8/Pebax MMM. A more detailed comparison of [EMIM][OAc]/CuBTC/Pebax MMMs with the other IL/MOF/polymer MMMs reported in the literature is given in Table S4 and results showed that CO_2 permeabilities and CO_2/N_2 selectivities of [EMIM][OAc]/-CuBTC/Pebax MMMs presented in this study are superior to the literature data reported to-date. To the best of our knowledge, CO_2 permeability of the [EMIM][OAc]/CuBTC/Pebax MMM with 15 wt.% [EMIM][OAc]/CuBTC filler loading was the highest among the values reported for other types of IL/MOF/Pebax MMMs while CO_2/N_2 selectivity was the highest among all IL/MOF/polymer MMMs reported in the literature as shown in Fig. 11. Hence, these results underscore the huge potential of IL-modified CuBTC composite for the fabrication of high-performance IL/MOF/polymer MMMs for CO_2/N_2 separation.

It is important for a membrane to maintain performance stability under continuous operating conditions, especially for industrial applications. Therefore, we tested the stability of [EMIM][OAc]/CuBTC/Pebax MMM with 15 wt.% [EMIM][OAc]/CuBTC loading under continuous operating conditions for up to 72 h. As shown in Fig. 12, CO_2 permeability and CO_2/N_2 selectivity fluctuated within a narrow range during this test. The test results demonstrated a good long-term working stability, indicating the structural stability of the synthesized [EMIM][OAc]/CuBTC/Pebax MMMs for gas separations. Furthermore, to validate the obtained results, another batch of IL/MOF/polymer MMM with 15 wt.% loading was prepared from scratch and tested for CO_2/N_2 gas separation. The obtained results (Fig. S4), CO_2 permeability of 301 ± 3.7 Barrer and CO_2/N_2 selectivity of 160 ± 10, were within ±5% error range, indicating the reproducibility of the MMMs. Overall, the results demonstrate the potential of IL/CuBTC/Pebax MMMs synthesized in this study, for continuous and extended operations.

4. Conclusion

CuBTC/Pebax MMMs and [EMIM][OAc]/CuBTC/Pebax MMMs were synthesized with 10, 15, and 20 wt.% loadings of CuBTC and [EMIM][OAc]/CuBTC fillers, respectively. Various experimental analysis showed that morphology of all the MMMs was homogenous and no apparent interfacial voids were observed, which can be ascribed to the well dispersion of CuBTC and [EMIM][OAc]/CuBTC fillers in the polymer matrix. At 15 wt.% [EMIM][OAc]/CuBTC loading, the MMM showed significantly higher CO_2 permeability of 335 Barrer and CO_2/N_2 selectivity of 176 compared to pure Pebax having a CO_2 permeability of 135 Barrer and CO_2/N_2 selectivity of 32. The CO_2 permeability and CO_2/N_2 selectivity of [EMIM][OAc]/CuBTC/Pebax MMM was 2.5- and 5.6-times higher than the pure Pebax membrane and significantly superior to the other IL/MOF/polymer MMMs reported in the literature under the same temperature and pressure conditions. All the CuBTC/Pebax MMMs and [EMIM][OAc]/CuBTC/Pebax MMMs that we synthesized in this work were found to be located above the Robeson's upper bound, indicating their exceptional performance for CO_2/N_2 separation. Considering the existence of a large number and variety of ILs, MOFs, and polymers, our results will contribute into the design and fabrication of new IL/MOF/polymer MMMs for various gas separations.

Author statement

Nitasha Habib: Methodology, Investigation, Writing - Original Draft, Writing - Review & Editing.

Ozce Durak: Methodology, Investigation, Writing - Original Draft, Writing - Review & Editing.

Muhammad Zeeshan: Methodology, Investigation.

Alper Uzun: Conceptualization, Supervision, Methodology, Writing - Original Draft, Writing - Review & Editing.

Seda Keskin: Conceptualization, Supervision, Methodology, Writing - Original Draft, Writing - Review & Editing.

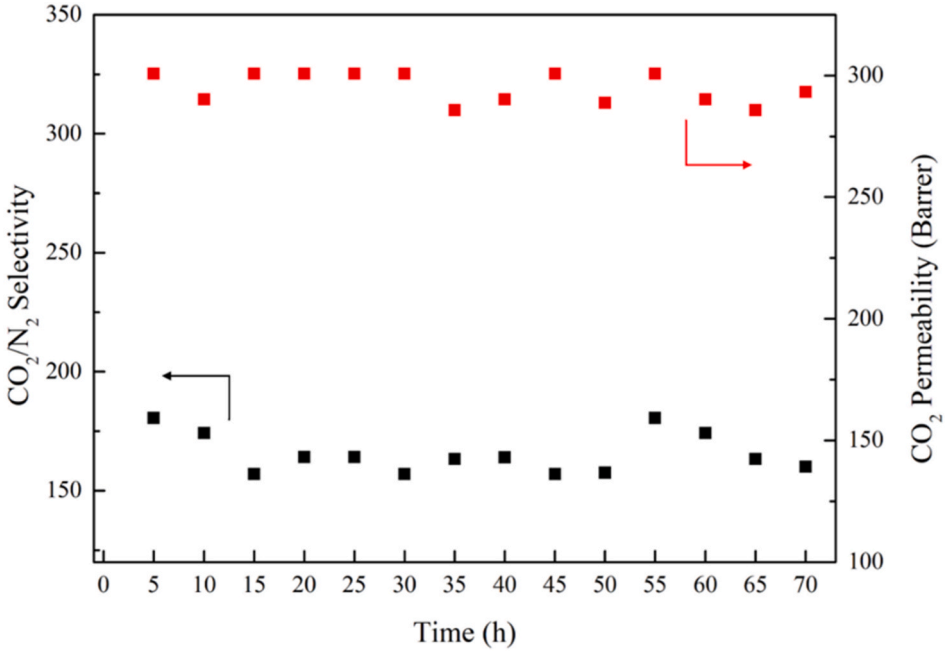


Fig. 12. Long-term stability of [EMIM][OAc]/CuBTC/Pebax MMM with 15 wt.% [EMIM][OAc]/CuBTC loading.

Declaration of competing interest

The authors declare that they have no known competing financial interests or personal relationships that could have appeared to influence the work reported in this paper.

Acknowledgements

S.K. acknowledges ERC-2017-Starting Grant. This study was also funded by the European Research Council under the European Union's Horizon 2020 research and innovation programme (ERC-2017-Starting Grant, grant agreement no. 756489-COSMOS). The authors gratefully acknowledge the support of Koç University TÜPRAŞ Energy Center (KUTEM), Koç University Surface Science and Technology Center (KUYTAM).

Appendix A. Supplementary data

Supplementary data to this article can be found online at https://doi.org/10.1016/j.memsci.2022.120712.

References

[1] N.N. Meis, J.H. Bitter, K.P. de Jong, Support and size effects of activated hydrotalcites for precombustion CO_2 capture, Ind. Eng. Chem. Res. 49 (3) (2010) 1229–1235.
[2] L.M. Robeson, The upper bound revisited, J. Membr. Sci. 320 (1–2) (2008) 390–400.
[3] G. Dong, H. Li, V. Chen, Challenges and opportunities for mixed-matrix membranes for gas separation, J. Mater. Chem. 1 (15) (2013) 4610–4630.
[4] A.L. Khan, N. Habib, M. Aslam, Metal Organic Frameworks-Based Mixed Matrix Membranes for Gas Separation, Nanomaterials for Air Remediation, Elsevier, 2020, pp. 273–292.
[5] N. Habib, Z. Shamair, N. Tara, A.-S. Nizami, F.H. Akhtar, N.M. Ahmad, M.A. Gilani, M.R. Bilad, A.L. Khan, Development of highly permeable and selective mixed matrix membranes based on Pebax® 1657 and NOTT-300 for CO_2 capture, Separ. Purif. Technol. 234 (2020), 116101.
[6] N. Tara, Z. Shamair, N. Habib, M. Craven, M.R. Bilad, M. Usman, X. Tu, A.L. Khan, Simultaneous increase in CO2 permeability and selectivity by BIT-72 and modified BIT-72 based mixed matrix membranes, Chem. Eng. Res. Des. 178 (2021) 136–147.
[7] Q. Qian, P.A. Asinger, M.J. Lee, G. Han, K. Mizrahi Rodriguez, S. Lin, F. M. Benedetti, A.X. Wu, W.S. Chi, Z.P. Smith, MOF-based membranes for gas separations, Chem. Rev. 120 (16) (2020) 8161–8266.
[8] S. Xu, H. Huang, X. Guo, Z. Qiao, C. Zhong, Highly selective gas transport channels in mixed matrix membranes fabricated by using water-stable Cu-BTC, Separ. Purif. Technol. 257 (2021), 117979.
[9] N. Tien-Binh, H. Vinh-Thang, X.Y. Chen, D. Rodrigue, S. Kaliaguine, Crosslinked MOF-polymer to enhance gas separation of mixed matrix membranes, J. Membr. Sci. 520 (2016) 941–950.
[10] A.F. Bushell, M.P. Attfield, C.R. Mason, P.M. Budd, Y. Yampolskii, L. Starannikova, A. Rebrov, F. Bazzarelli, P. Bernardo, J.C. Jansen, Gas permeation parameters of mixed matrix membranes based on the polymer of intrinsic microporosity PIM-1 and the zeolitic imidazolate framework ZIF-8, J. Membr. Sci. 427 (2013) 48–62.
[11] Y. Wang, G. Yang, H. Guo, X. Meng, G. Kong, Z. Kang, R. Guillet-Nicolas, S. Mintova, Preparation of HKUST-1/PEI mixed-matrix membranes: adsorption-diffusion coupling control of small gas molecules, J. Membr. Sci. 643 (2022), 120070.
[12] R. Thür, N. Van Velthoven, S. Slootmaekers, J. Didden, R. Verbeke, S. Smolders, M. Dickmann, W. Egger, D. De Vos, I.F. Vankelecom, Bipyridine-based UiO-67 as novel filler in mixed-matrix membranes for CO_2-selective gas separation, J. Membr. Sci. 576 (2019) 78–87.
[13] N. Tien-Binh, D. Rodrigue, S. Kaliaguine, In-situ cross interface linking of PIM-1 polymer and UiO-66-NH_2 for outstanding gas separation and physical aging control, J. Membr. Sci. 548 (2018) 429–438.
[14] M.Z. Ahmad, M. Navarro, M. Lhotka, B. Zornoza, C. Téllez, W.M. de Vos, N. E. Benes, N.M. Konnertz, T. Visser, R. Semino, Enhanced gas separation performance of 6FDA-DAM based mixed matrix membranes by incorporating MOF UiO-66 and its derivatives, J. Membr. Sci. 558 (2018) 64–77.
[15] T. Wu, N. Prasetya, K. Li, Recent advances in aluminium-based metal-organic frameworks (MOF) and its membrane applications, J. Membr. Sci. 615 (2020), 118493.
[16] M.S. Buddin, A. Ahmad, A review on metal-organic frameworks as filler in mixed matrix membrane: recent strategies to surpass upper bound for CO_2 separation, J. CO2 Util. 51 (2021), 101616.
[17] V. Nafisi, M.-B. Hägg, Development of dual layer of ZIF-8/PEBAX-2533 mixed matrix membrane for CO_2 capture, J. Membr. Sci. 459 (2014) 244–255.
[18] M.J.C. Ordonez, K.J. Balkus Jr., J.P. Ferraris, I.H. Musselman, Molecular sieving realized with ZIF-8/Matrimid® mixed-matrix membranes, J. Membr. Sci. 361 (1–2) (2010) 28–37.
[19] F.P. Kinik, A. Uzun, S. Keskin, Ionic liquid/metal–organic framework composites: from synthesis to applications, ChemSusChem 10 (14) (2017) 2842–2863.
[20] O. Durak, M. Zeeshan, N. Habib, H.C. Gülbalkan, A.A.A.M. Alsuhile, H.P. Çağlayan, S.F. Kurtoğlu-Öztulum, Y. Zhao, Z.P. Haşlak, A. Uzun, Composites of porous materials with ionic liquids: synthesis, characterization, applications, and beyond, Microporous Mesoporous Mater. (2022), 111703.
[21] M. Zeeshan, V. Nozari, M.B. Yagci, T. Isık, U. Unal, V. Ortalan, S. Keskin, A. Uzun, Core–shell type ionic liquid/metal organic framework composite: an exceptionally high CO_2/CH_4 selectivity, J. Am. Chem. Soc. 140 (32) (2018) 10113–10116.
[22] M. Zeeshan, S. Keskin, A. Uzun, Enhancing CO_2/CH_4 and CO_2/N_2 separation performances of ZIF-8 by post-synthesis modification with [BMIM][SCN], Polyhedron 155 (2018) 485–492.
[23] H.M. Polat, M. Zeeshan, A. Uzun, S. Keskin, Unlocking CO_2 separation performance of ionic liquid/CuBTC composites: combining experiments with molecular simulations, Chem. Eng. J. 373 (2019) 1179–1189.
[24] M. Zeeshan, H. Kulak, S. Kavak, H.M. Polat, O. Durak, S. Keskin, A. Uzun, Influence of anion size and electronic structure on the gas separation performance of ionic liquid/ZIF-8 composites, Microporous Mesoporous Mater. 306 (2020), 110446.
[25] F.P. Kinik, C. Altintas, V. Balci, B. Koyuturk, A. Uzun, S. Keskin, [BMIM][PF_6] incorporation doubles CO_2 selectivity of ZIF-8: elucidation of interactions and their consequences on performance, ACS Appl. Mater. Interfaces 8 (45) (2016) 30992–31005.
[26] B. Koyuturk, C. Altintas, F.P. Kinik, S. Keskin, A. Uzun, Improving gas separation performance of ZIF-8 by [BMIM][BF_4] incorporation: interactions and their consequences on performance, J. Phys. Chem. C 121 (19) (2017) 10370–10381.
[27] W. Chen, Z. Zhang, C. Yang, J. Liu, H. Shen, K. Yang, Z. Wang, PIM-based mixed-matrix membranes containing MOF-801/ionic liquid nanocomposites for enhanced CO_2 separation performance, J. Membr. Sci. 636 (2021), 119581.
[28] I.C. Ferreira, T.J. Ferreira, A.D. Barbosa, B. de Castro, R.P. Ribeiro, J.P. Mota, V. D. Alves, L. Cunha-Silva, I.A. Esteves, L.A. Neves, Cr-based MOF/IL composites as fillers in mixed matrix membranes for CO_2 separation, Separ. Purif. Technol. 276 (2021), 119303.
[29] Y. Ban, Z. Li, Y. Li, Y. Peng, H. Jin, W. Jiao, A. Guo, P. Wang, Q. Yang, C. Zhong, Confinement of ionic liquids in nanocages: tailoring the molecular sieving properties of ZIF-8 for membrane-based CO_2 capture, Angew. Chem. Int. Ed. 54 (51) (2015) 15483–15487.
[30] H. Li, L. Tuo, K. Yang, H.-K. Jeong, Y. Dai, G. He, W. Zhao, Simultaneous enhancement of mechanical properties and CO_2 selectivity of ZIF-8 mixed matrix membranes: interfacial toughening effect of ionic liquid, J. Membr. Sci. 511 (2016) 130–142.
[31] I. Yasmeen, A. Ilyas, Z. Shamair, M.A. Gilani, S. Rafiq, M.R. Bilad, A.L. Khan, Synergistic effects of highly selective ionic liquid confined in nanocages: exploiting the three component mixed matrix membranes for CO_2 capture, Chem. Eng. Res. Des. 155 (2020) 123–132.
[32] R. Lin, L. Ge, H. Diao, V. Rudolph, Z. Zhu, Ionic liquids as the MOFs/polymer interfacial binder for efficient membrane separation, ACS Appl. Mater. Interfaces 8 (46) (2016) 32041–32049.
[33] J.H. Kim, Y.M. Lee, Gas permeation properties of poly (amide-6-b-ethylene oxide)–silica hybrid membranes, J. Membr. Sci. 193 (2) (2001) 209–225.
[34] I. Pinnau, B. Freeman, Formation and modification of polymeric membranes: overview, ACS (Am. Chem. Soc.) Symp. Ser. 744 (2000) 1–22.
[35] M.Z. Ahmad, T.A. Peters, N.M. Konnertz, T. Visser, C. Téllez, J. Coronas, V. Fila, W. M. de Vos, N.E. Benes, High-pressure CO_2/CH_4 separation of Zr-MOFs based mixed matrix membranes, Separ. Purif. Technol. 230 (2020), 115858.
[36] J. Ahn, W.-J. Chung, I. Pinnau, J. Song, N. Du, G.P. Robertson, M.D. Guiver, Gas transport behavior of mixed-matrix membranes composed of silica nanoparticles in a polymer of intrinsic microporosity (PIM-1), J. Membr. Sci. 346 (2) (2010) 280–287.
[37] M.M. Zagho, M.K. Hassan, M. Khraisheh, M.A.A. Al-Maadeed, S. Nazarenko, A review on recent advances in CO_2 separation using zeolite and zeolite-like materials as adsorbents and fillers in mixed matrix membranes (MMMs), Chemical Engineering Journal Advances 6 (2021), 100091.
[38] V. Bondar, B. Freeman, I. Pinnau, Gas transport properties of poly (ether-b-amide) segmented block copolymers, J. Polym. Sci. B Polym. Phys. 38 (15) (2000) 2051–2062.
[39] A. Klamt, F. Eckert, W. Arlt, COSMO-RS: an alternative to simulation for calculating thermodynamic properties of liquid mixtures, Ann. Rev. Chem. Biomol. Eng. 1 (2010) 101–122.
[40] S. Lee, J.H. Lee, J. Kim, User-friendly graphical user interface software for ideal adsorbed solution theory calculations, Kor. J. Chem. Eng. 35 (1) (2018) 214–221.
[41] V. Nozari, M. Zeeshan, S. Keskin, A. Uzun, Effect of methylation of ionic liquids on the gas separation performance of ionic liquid/metal–organic framework composites, CrystEngComm 20 (44) (2018) 7137–7143.
[42] Ö. Durak, H. Kulak, S. Kavak, H.M. Polat, S. Keskin, A. Uzun, Towards complete elucidation of structural factors controlling thermal stability of IL/MOF composites: effects of ligand functionalization on MOFs, J. Phys. Condens. Matter 32 (48) (2020), 484001.
[43] O. Durak, M. Zeeshan, S. Keskin, A. Uzun, [BMIM][OAc] coating layer makes activated carbon almost completely selective for CO_2, Chem. Eng. J. 437 (2022), 135436.
[44] R. Mahugo, A. Mayoral, M. Sánchez-Sánchez, I. Diaz, Observation of Ag nanoparticles in/on Ag@ MIL-100 (Fe) prepared through different procedures, Front. Chem. 7 (2019) 686.
[45] K.B. Sezginel, S. Keskin, A. Uzun, Tuning the gas separation performance of CuBTC by ionic liquid incorporation, Langmuir 32 (4) (2016) 1139–1147.

[46] A. Jalal, Y. Zhao, A. Uzun, Pyrolysis temperature tunes the catalytic properties of CuBTC-derived carbon-embedded copper catalysts for partial hydrogenation, Ind. Eng. Chem. Res. 61 (5) (2022) 2068–2080.
[47] M. Zeeshan, V. Nozari, S. Keskin, A. Uzun, Structural factors determining thermal stability limits of ionic liquid/MOF composites: imidazolium ionic liquids combined with CuBTC and ZIF-8, Ind. Eng. Chem. Res. 58 (31) (2019) 14124–14138.
[48] L. Lei, A. Lindbråthen, M. Sandru, M.T.G. Gutierrez, X. Zhang, M. Hillestad, X. He, Spinning cellulose hollow fibers using 1-ethyl-3-methylimidazolium acetate–dimethylsulfoxide co-solvent, Polymers 10 (9) (2018) 972.
[49] Y. Huang, Y. Xiao, H. Huang, Z. Liu, D. Liu, Q. Yang, C. Zhong, Ionic liquid functionalized multi-walled carbon nanotubes/zeolitic imidazolate framework hybrid membranes for efficient H_2/CO separation, Chem. Commun. 51 (97) (2015) 17281–17284.
[50] Y.-K. Seo, G. Hundal, I.T. Jang, Y.K. Hwang, C.-H. Jun, J.-S. Chang, Microwave synthesis of hybrid inorganic–organic materials including porous $Cu_3(BTC)_2$ from Cu (II)-trimesate mixture, Microporous Mesoporous Mater. 119 (1–3) (2009) 331–337.
[51] M. Zeeshan, H.C. Gulbalkan, Z.P. Haslak, S. Keskin, A. Uzun, Doubling CO_2/N_2 separation performance of CuBTC by incorporation of 1-n-ethyl-3-methylimidazolium diethyl phosphate, Microporous Mesoporous Mater. 316 (2021), 110947.
[52] M. Li, X. Zhang, S. Zeng, H. Gao, J. Deng, Q. Yang, S. Zhang, Pebax-based composite membranes with high gas transport properties enhanced by ionic liquids for CO_2 separation, RSC Adv. 7 (11) (2017) 6422–6431.
[53] L. Xiang, Y. Pan, G. Zeng, J. Jiang, J. Chen, C. Wang, Preparation of poly (ether-block-amide)/attapulgite mixed matrix membranes for CO_2/N_2 separation, J. Membr. Sci. 500 (2016) 66–75.
[54] B. Ge, Y. Xu, H. Zhao, H. Sun, Y. Guo, W. Wang, High performance gas separation mixed matrix membrane fabricated by incorporation of functionalized submicrometer-sized metal-organic framework, Materials 11 (8) (2018) 1421.
[55] S. Charati, A. Houde, S. Kulkarni, M. Kulkarni, Transport of gases in aromatic polyesters: correlation with WAXD studies, J. Polym. Sci. B Polym. Phys. 29 (8) (1991) 921–931.
[56] B. Monteiro, A.R. Nabais, F.A. Almeida Paz, L. Cabrita, L.C. Branco, I.M. Marrucho, L.A. Neves, C.C. Pereira, Membranes with a low loading of metal–organic framework-supported ionic liquids for CO_2/N_2 separation in CO_2 capture, Energy Technol. 5 (12) (2017) 2158–2162.
[57] Y. Wang, J. Ren, M. Deng, Ultrathin solid polymer electrolyte PEI/Pebax2533/$AgBF_4$ composite membrane for propylene/propane separation, Separ. Purif. Technol. 77 (1) (2011) 46–52.
[58] N. Azizi, M.R. Hojjati, M.M. Zarei, Study of CO_2 and CH_4 permeation properties through prepared and characterized blended Pebax-2533/PEG-200 membranes, Silicon 10 (4) (2018) 1461–1467.
[59] A. Ghadimi, M. Amirilargani, T. Mohammadi, N. Kasiri, B. Sadatnia, Preparation of alloyed poly (ether block amide)/poly (ethylene glycol diacrylate) membranes for separation of CO_2/H_2 (syngas application), J. Membr. Sci. 458 (2014) 14–26.
[60] R.S. Murali, A. Ismail, M. Rahman, S. Sridhar, Mixed matrix membranes of Pebax-1657 loaded with 4A zeolite for gaseous separations, Separ. Purif. Technol. 129 (2014) 1–8.
[61] B. Molki, W.M. Aframehr, R. Bagheri, J. Salimi, Mixed matrix membranes of polyurethane with nickel oxide nanoparticles for CO_2 gas separation, J. Membr. Sci. 549 (2018) 588–601.
[62] F.P. Kinik, C. Altintas, V. Balci, B. Koyuturk, A. Uzun, S. Keskin, [BMIM][PF_6] incorporation doubles CO_2 selectivity of ZIF-8: elucidation of interactions and their consequences on performance, ACS Appl. Mater. Interfaces 8 (45) (2016) 30992–31005.
[63] J. Shen, G. Liu, K. Huang, Q. Li, K. Guan, Y. Li, W. Jin, UiO-66-polyether block amide mixed matrix membranes for CO_2 separation, J. Membr. Sci. 513 (2016) 155–165.
[64] M. Aroon, A. Ismail, T. Matsuura, M. Montazer-Rahmati, Performance studies of mixed matrix membranes for gas separation: a review, Separ. Purif. Technol. 75 (3) (2010) 229–242.
[65] Z. Ziobrowski, A. Rotkegel, Enhanced CO_2/N_2 separation by supported ionic liquid membranes (SILMs) based on PDMS and 1-ethyl-3-methylimidazolium acetate, Chem. Eng. Commun. 208 (1) (2021) 137–147.
[66] T.T. Moore, W.J. Koros, Non-ideal effects in organic–inorganic materials for gas separation membranes, J. Mol. Struct. 739 (1–3) (2005) 87–98.
[67] Z. Guo, W. Zheng, X. Yan, Y. Dai, X. Ruan, X. Yang, X. Li, N. Zhang, G. He, Ionic liquid tuning nanocage size of MOFs through a two-step adsorption/infiltration strategy for enhanced gas screening of mixed-matrix membranes, J. Membr. Sci. 605 (2020), 118101.